Leakage Currents Mechanism in Thin Films of Ferroelectric $Hf_{0.5}Zr_{0.5}O_2$

D. R. Islamov[a,b], A. G. Chernikova[c], M. G. Kozodaev[c], T. V. Perevalov[a,b], V. A. Gritsenko[a,b], O. M. Orlov[d], and A. V. Markeev[c]

[a] Rzhanov Institute of Semiconductor Physics SB RAS, Novosibirsk 630090, Russian Federation
[b] Novosibirsk State University, Novosibirsk 630090, Russian Federation
[c] Moscow Institute of Physics and Technology, Dolgoprudny 141700, Russian Federation
[d] JSC Molecular Electronics Research Institute, Zelenograd 124460, Russian Federation

We study the charge transport mechanism in ferroelectric $Hf_{0.5}Zr_{0.5}O_2$ thin films. Transport properties of the leakage currents in $Hf_{0.5}Zr_{0.5}O_2$ are described by phonon-assisted tunneling between traps. Comparison with transport properties of amorphous $Hf_{0.5}Zr_{0.5}O_2$ demonstrates that the transport mechanism does not depend on the crystal structure. The thermal trap energy of 1.25 eV and optical trap energy of 2.5 eV in $Hf_{0.5}Zr_{0.5}O_2$ were determined based on comparison of experimentally measured data on transport with simulations within phonon-assisted tunneling between traps in dielectric films. We found that the trap density in ferroelectric $Hf_{0.5}Zr_{0.5}O_2$ is slightly less that one in amorphous $Hf_{0.5}Zr_{0.5}O_2$. A hypothesis that oxygen vacancies are responsible for the charge transport in $Hf_{0.5}Zr_{0.5}O_2$ is confirmed by electronic structure *ab initio* simulation.

Introduction

Hafnia (HfO_2) was considered as a paraelectric material until observation of ferroelectric effect in thin films of doped HfO_2 after high-temperature annealing (~1000 °C) (1), (2). Of particular interest is the fact that ferroelectricity was also demonstrated in thin of the solid solution $Hf_{0.5}Zr_{0.5}O_2$ which requires annealing at significantly lower temperatures (3)–(6). Ferroelectricity in these materials is associated with the ability to stabilize noncentrosymmetric orthorhombic phase $Pbc2_1$ (4). We should note that the hafnia-based materials have a number of advantages over conventional ferroelectric regarding compatibility with technological processes used in microelectronics, and has already demonstrated their ability to provide very high elements density. Taking into account advantages of the ferroelectric random access memory (FeRAM) as non-volatile, high-speed performance, high number of switching cycles, the discovery of ferroelectric effect in hafnia-based materials gave an impetus for development of universal memory concept, which may lead to a significant breakthrough in the development of memory devices (7).

An unsolved problem in the way of development of FeRAM-based universal memory is the spontaneous depolarization of the active medium, which leads to short data storage time (retention) that is observed in Ref. (8). One of the possible reason of spontaneous depolarization is leakage currents through the ferroelectric thin films. High-κ $Hf_{0.5}Zr_{0.5}O_2$ thin films (κ>16 depending on structure phase) can be used as sub-gate dielectrics in MOSFET and FinFET transistors instead of SiO_2. Thus, it is very important to know

charge transport mechanisms in thin dielectrics films to control the leakage currents for development of high quality memory devices. Purpose of the present work is to study charge transport mechanism in ferroelectric $Hf_{0.5}Zr_{0.5}O_2$.

Experiment details

Transport measurements were performed for TiN/$Hf_{0.5}Zr_{0.5}O_2$/Pt metal/insulator/metal (MIM) structures. Test structure were fabricated with atomic layer deposition (ALD) technique. The 10-nm-thick TiN layer was deposited on oxidized Si (100) substrate. Then the 10-nm-thick $Hf_{0.5}Zr_{0.5}O_2$ films we deposited at 240 °C from Tetrakis(EthylMethylAmino)Hafnium (TEMAHf), Tetrakis(EthylMethylAmino)Zirconium (TEMAZr), and H_2O, as the Hf-precursor, Zr-precursor, and oxygen source, respectively. The TEMAHf and TEMAZr precursors were mixed in single-cocktail balloon. Laser ellipsometry and Rutherford backscattering spectroscopy confirmed the thickness and stoichiometry of as deposited $Hf_{0.5}Zr_{0.5}O_2$ films. A part of samples was annealed at 400 °C in N_2 environment during 30 sec (rapid thermal annealing, RTA). The crystalline structures of as deposited and annealed films were examined by symmetrical X-Ray diffraction (XRD) using ARL X'TRA tool (Thermo Scientific) utilizing Cu*K*α radiation. For transport measurements, the Pt top electrodes (thickness of ~30 nm) were deposited through shadow mask with round holes (area is 7.1×10^4 μm^2) by electron beam evaporation on as deposited $Hf_{0.5}Zr_{0.5}O_2$ films and after RTA treatment.

The DC current-voltage (*I-V*) curves were measured using Agilent B1500A Semiconductor device parameter analyzer at temperatures of 25–175 °C. Polarization-voltage (*P-V*) curves were obtained by integration of displacement current response in reply to the stepped triangle voltage. The leakage current was subtracted from the current response in order to eliminate the polarization and displacement current contributions.

The electronic structure of $Hf_{0.5}Zr_{0.5}O_2$ was calculated within the spin polarized density functional theory using the *ab initio* simulation code Quantum ESPRESSO with B3LYP hybrid exchange-correlation functional (9). The oxygen vacancy (V_O) was generated by the removal of an O atom, followed by relaxation of remaining atoms in 96-atom supercell.

Results and discussions

The XRD spectra of as deposited and annealed films are presented in Figure 1 by black and gray lines, respectively. The range of 2θ was chosen due to the highest intensity of the response related to the $Hf_{0.5}Zr_{0.5}O_2$. The XRD spectra of $Hf_{0.5}Zr_{0.5}O_2$ films show that as deposited films demonstrate amorphous structure (a-$Hf_{0.5}Zr_{0.5}O_2$), while annealed films are polycrystalline with monoclinic $P2_1/c$ (peaks near 28.5° and 31.6°) tetragonal $P4_2/nmc$ (30.8°), and noncentralsymmetric orthorhombic $Pbc2_1$ (30.5°) phases. The presence of ferroelectric properties of f-$Hf_{0.5}Zr_{0.5}O_2$ films after RTA is confirmed by direction of *I-V* hysteresis (dashed arrows in Figure 2) and by observing peaks on *I-V* characteristics (dashed arrows in Figure 2) and characteristic hysteresis on the *P-V* plate for Pt/f-$Hf_{0.5}Zr_{0.5}O_2$/TiN structures, as shown in Figure 3.

Figure 4 shows results of *ab initio* calculations performed for four types of oxygen vacancy in orthorhombic $Hf_{0.5}Zr_{0.5}O_2$ ($Pbc2_1$). The calculated partial density of states (PDOS) of oxygen, hafnium and zirconium atoms for all types of neutral oxygen vacancies V_O in $Hf_{0.5}Zr_{0.5}O_2$ are shown in Figures 4(a)-(d). ZrZr=V_O-Hf and HfHf=V_O-Zr

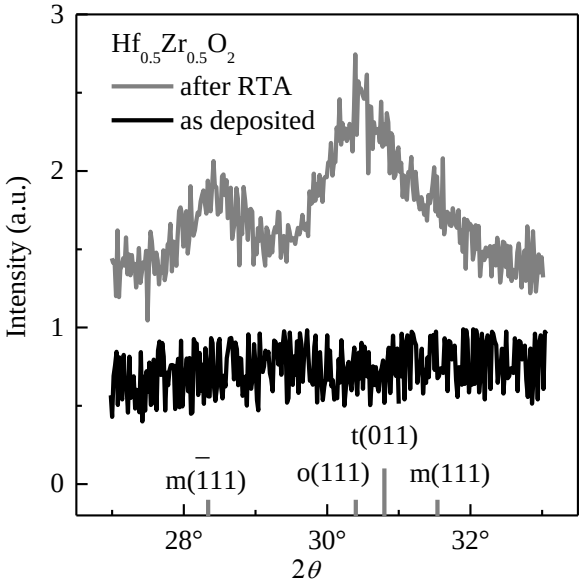

Figure 1. XRD spectra of as deposited a-$Hf_{0.5}Zr_{0.5}O_2$ and f-$Hf_{0.5}Zr_{0.5}O_2$ after RTA.

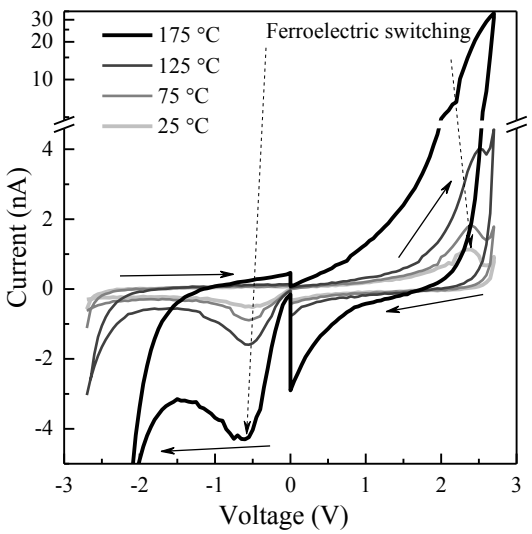

Figure 2. Experimental current-voltage characteristics for Pt/f-$Hf_{0.5}Zr_{0.5}O_2$/TiN structures at different temperatures.

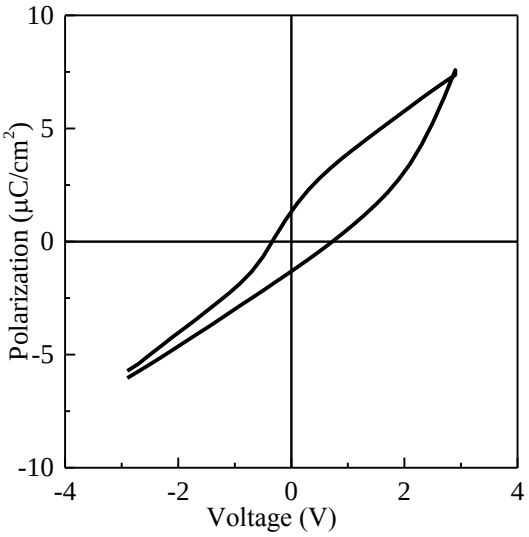

Figure 3. Polarization-voltage characteristics for Pt/f-$Hf_{0.5}Zr_{0.5}O_2$/TiN structures at room temperature.

represent threefold oxygen vacancies with 2Zr+Hf and 2Hf+Zr metal atoms around, while HfHf=V_O=ZrZr and HfZr=V_O=HfZr represent fourfold oxygen vacancies with different spatial arrangement of Hf and Zr atoms around the vacancy. The schematic spatial configurations of the defects are shown in the insets of the Fig. 4(a)-(d). We can see that the electronic structures of the different-type oxygen vacancies in $Hf_{0.5}Zr_{0.5}O_2$ are similar: threefold and fourfold coordinated vacancies form filled states in the band gap of 3.4 eV and 2.7 eV above the valence band, respectively. The nearest metal atoms to the oxygen vacancy give the most contribution to the defect states as shown in Figs. 4(a)-(d). The next most important contribution to the defect state is given by the nearest to the oxygen vacancy atoms. The contribution of those far from V_O atoms is negligible. Calculated Kohn-Sham energy levels for the oxygen vacancies in different charge states are shown in Figs. 4(e) and 4(f). We can see that a trapped on the defect electron (V_O^{-1})

has an energy of ~1 eV below the bottom of the conduction band E_c. Trapping a hole (V_O^{+1}) leads to a descent of the energy level compared to neutral oxygen vacancy V_O. Thus, one can conclude that the defect states in the band gap are localized, and the oxygen vacancies can act as a trap for electrons, as well as for holes, being involved in the charge transport.

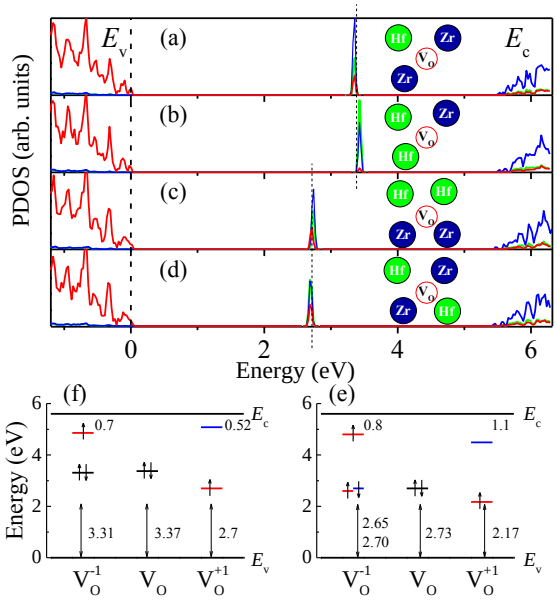

Figure 4. The calculated partial density of states (PDOS) of oxygen (red lines), hafnium (blue lines) and zirconium (green lines) atoms for all types of neutral oxygen vacancies V_O in $Hf_{0.5}Zr_{0.5}O_2$: (a) ZrZr=V_O-Hf, (b) HfHf=V_O-Zr, (c) HfHf=V_O=ZrZr, (d) HfZr=V_O=HfZr. The energy levels of HfHf=V_O-Zr-type (f) and HfHf=V_O=ZrZr-type (e) oxygen vacancy in different charge states: V_O^{-1} negatively charged state, V_O^{+1} positively charged state. Black horizontal lines show filled states with the total zero spin; red lines correspond to up-spin states, blue lines – down-spin states. The electron spins localized on the defect are shown with arrows. The energy distance between energy levels and the top of the valence band (in eV) are shown by bilateral arrows. The reference point is the top of valence band E_v=0.

Despite that *ab initio* calculations predict amphoteric nature of traps, the capacitance-voltage measurements on trapped charge accumulation demonstrate that mostly holes are involving in transport processes (10). Thus, further transport analysis we will perform in terms of monopolar (namely, hole) conductivity.

Figure 5 shows experimental current-voltage dependencies (characters) of leakage current contribution for Pt/f-$Hf_{0.5}Zr_{0.5}O_2$/TiN MIM structure at different temperatures *T* on semi log plate (*I-V-T*). The current depends on the voltage and temperature exponentially. Well-known model of the charge transport in dielectrics is the Frenkel model of isolated trap ionization (11), (12). This model can describe experimental *I-V-T* dependencies using overestimated value of dynamic permittivity (ε_∞ = 6) with respect to predicted by *ab initio* calculations (ε_∞ = 4.8) and underestimated value of frequency factor $v << W/h$ (*W* is trap energy; *h* is the Planck constant). Followed by Refs. (10), (11),

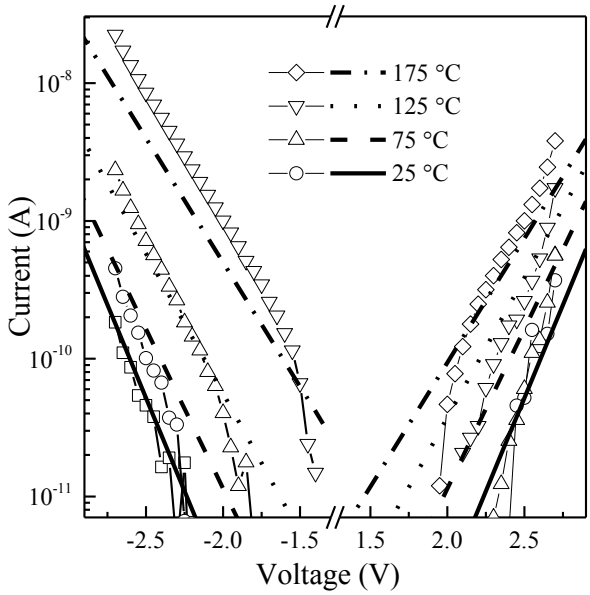

Figure 5. Experimental (characters) current-voltage characteristics and simulations (lines) for Pt/f-$Hf_{0.5}Zr_{0.5}O_2$/TiN structures at different temperatures.

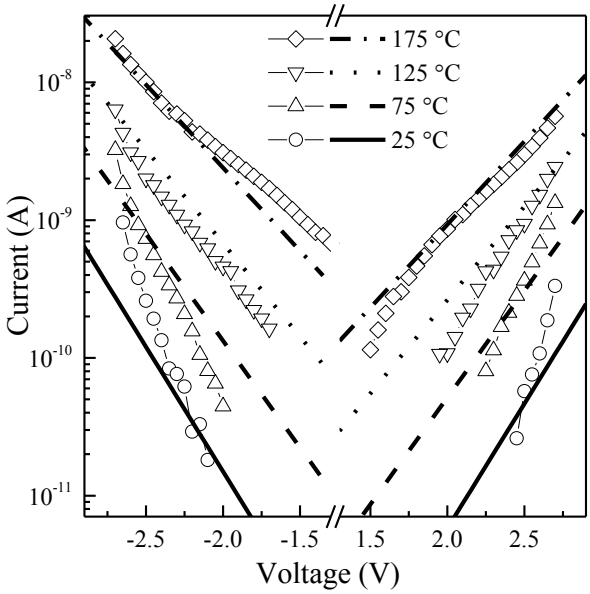

Figure 6. Experimental (characters) current-voltage characteristics and simulations (lines) for Pt/a-$Hf_{0.5}Zr_{0.5}O_2$/TiN structures at different temperatures.

we analyzed experimentally measured current-voltage characteristics of Pt/f-$Hf_{0.5}Zr_{0.5}O_2$/TiN structures in terms of phonon-assisted tunneling between traps (12). The current density *J* within this framework is described as follows:

$$J = \frac{e\gamma}{s^2},$$
$$\gamma = \frac{\sqrt{2\pi}\hbar W_t}{m^* s^2 \sqrt{kT(W_{opt} - W_t)}} \exp\left(-\frac{W_{opt} - W_t}{2kT}\right) \exp\left(-\frac{2s\sqrt{2m^* W_t}}{\hbar}\right) \sinh\left(\frac{eFs}{2kT}\right), \quad [1]$$

where e is the elementary charge, s is the mean distance between traps, γ is the probability rate of charge carrier tunneling between traps, $\hbar = h/2\pi$, W_t is thermal trap energy, W_{opt} is optical energy of the trap, m^* is the effective mass, k is the Boltzmann constant, F is the electric field in the dielectric medium. Phonon-assisted tunneling between traps describes experimental *I-V-T* with very good quantitative agreement with thermal and optical trap energies W_t=1.25eV and W_{opt}=2.5eV, respectively, $m^* = (0.24\pm0.02)\, m_0$ (hereby m_0 is the free electron mass), trap density $N = s^{-3} = 3\times10^{19}$ cm^{-3} (lines on Fig. 4). Some deviations of calculations from experimental data might be caused by simplification of used model. Full model involves non-static 3D Shockley-Read-Hall with Poison equations with boundary conditions on metal electrodes. We used 1D simple model here to show the main charge transport mechanism of leakage currents through the dielectric films. Also, it should be noted that the leakage currents might be associated with any of m-, t- and o-$Hf_{0.5}Zr_{0.5}O_2$ phases that present in our samples with ferroelectric properties.

The same procedure was applied for Pt/a-$Hf_{0.5}Zr_{0.5}O_2$/TiN structures with amorphous films. Figure 6 shows comparing of experimentally measured current-voltage characteristics for Pt/a-$Hf_{0.5}Zr_{0.5}O_2$/TiN structures at different temperatures with calculated ones in terms of phonon-assisted tunneling between traps [1]. The best agreement of calculated curves with experimental data was got with the following parameter values: W_t=1.25eV, W_{opt}=2.5eV, $m^* = (0.34\pm0.02)\, m_0$, $N = 1\times10^{20}$ cm^{-3}. We should note that obtained values of trap energies are the same as for amorphous a-$Hf_xZr_{1-x}O_y$, synthesized by different techniques (e.g., by physical vapor deposition) (10).

As far as thermal and optical energies for amorphous and ferroelectric $Hf_{0.5}Zr_{0.5}O_2$ films do not depend on crystal phase, one can assume that the traps in different phases of these films have the same nature. Recently it was shown that the oxygen vacancies act as the charge traps in hafnium oxide (11). At the same time, thermal and optical trap energies in HfO_2 have values of 1.25 eV and 2.5 eV, respectively. Taking into account, that the oxygen vacancies in HfO_2 and ZrO_2 have the same electronic structure, the fact that $Hf_{0.5}Zr_{0.5}O_2$ is the solid solution of these oxides, and that the trap energies in HfO_2 have the same values as in $Hf_{0.5}Zr_{0.5}O_2$, one can assume that the oxygen vacancies act as the charge traps in a-$Hf_{0.5}Zr_{0.5}O_2$ and f-$Hf_{0.5}Zr_{0.5}O_2$ (13), (14). Thus, we conclude that the leakage currents mechanism in $Hf_{0.5}Zr_{0.5}O_2$ does not depend on crystal structure of $Hf_{0.5}Zr_{0.5}O_2$ films and is phonon-assisted tunneling between oxygen vacancies. The only difference is charge trap density, which is lower in f-$Hf_{0.5}Zr_{0.5}O_2$ (3×10^{19}cm^{-3} with respect to 1×10^{20}cm^{-3} in a-$Hf_{0.5}Zr_{0.5}O_2$).

Summary

In conclusion, this study demonstrates that the charge transport of amorphous and ferroelectric $Hf_{0.5}Zr_{0.5}O_2$ films is described by phonon-assisted tunneling between traps. Comparing experimental current-voltage characteristics with results of simulations revealed energy parameters of the charge traps in $Hf_{0.5}Zr_{0.5}O_2$: the thermal trap energy of 1.25 eV and the optical trap energy of 2.5 eV do not depend on the crystal phase and are

equal to that for HfO_2 and ZrO_2. Equality of trap energy values with ones in HfO_2 and ZrO_2 allows one to conclude that the traps are oxygen vacancies. A hypothesis that oxygen vacancies are responsible for the charge transport in $Hf_{0.5}Zr_{0.5}O_2$ is confirmed by electronic structure *ab initio* simulation. Reported results agree with recently published data on study of charge transport in amorphous $Hf_{0.5}Zr_{0.5}O_2$, produced by other deposition techniques too, e. g., by physical vapor deposition (PVD) (10).

Acknowledgments

The work was supported by the Ministry of Education and Science of the Russian Federation (project #RFMEFI57614X0065).

References

1. T.S. Böscke, J. Müller, D. Bräuhaus *et al.*, *Appl. Phys. Lett.* **99**, 102903 (2011).
2. S. Mueller, J. Mueller, A. Singh *et al.*, *Adv. Function. Mater.* **22**, 2412 (2012).
3. J. Müller, T.S. Böscke, D. Bräuhaus *et al.*, *Appl. Phys. Lett.* **99**, 112901 (2011).
4. J. Müller, T.S. Böscke, U. Schröder *et al.*, *Nano Lett.* **12**, 4318 (2012).
5. M.H. Park, H.J. Kim, Y.J. Kim *et al.*, *Appl. Phys. Lett.* **102**, 112914 (2013).
6. A. Chernikova, M. Kozodaev, A. Markeev *et al.*, *Microelectron. Eng.* **147**, 15 (2015).
7. M.H. Park, Y.H. Lee, H.J. Kim *et al.*, *Adv. Mater.* **27**, 1811 (2015).
8. C.-H. Cheng and A. Chin, *IEEE Electron Dev. Lett.* **35**, 138 (2014).
9. P. Giannozzi et al., *J. Phys.: Condens. Matter* **21**, 395502 (2009).
10. D.R. Islamov, T.V. Perevalov, V.A. Gritsenko *et al.*, *Appl. Phys. Lett.* **106**, 102906 (2015).
11. D.R. Islamov, V.A. Gritsenko, C.H. Cheng and A. Chin, *Appl. Phys. Lett.* **105**, 222901 (2014).
12. K. A. Nasyrov and V. A. Gritsenko, *J. Appl. Phys.* **109**, 093705 (2011).
13. T.V. Perevalov, V.S. Aliev, V.A. Gritsenko *et al.*, *Appl. Phys. Lett.* **104**, 071904 (2014).
14. T.V. Perevalov, D.V. Gulyaev, V.S. Aliev *et al.*, *J. Appl. Phys.* **116**, 244109 (2014).